QUANTIFYING THE STRENGTHS OF DUAL-HYDROGEN-BOND DONORS AS ORGANOCATALYSTS

An Undergraduate Research Scholars Thesis

by

JACQUELINE SHEA

Submitted to the Undergraduate Research Scholars program
Texas A&M University
in partial fulfillment of the requirements for the designation as an

UNDERGRADUATE RESEARCH SCHOLAR

Approved by
Research Advisor: Dr. Steven E. Wheeler

May 2016

Major: Chemistry

TABLE OF CONTENTS

ABSTRACT

Quantifying the Strengths of Dual-Hydrogen-Bond Donors as Organocatalysts

Jacqueline Shea
Department of Chemistry
Texas A&M University

Research Advisor: Dr. Steven E. Wheeler
Department of Chemistry

Despite the importance of dual-hydrogen-bonding organocatalysis in modern synthetic organic chemistry, the optimal hydrogen-bond donors for various common functional groups remain unknown. Additionally, the relationship between the ability of a given organocatalyst to form strong hydrogen bonds with the substrate and the resulting catalytic activity is unclear. These relationships can be studied with density functional theory (DFT) to quantify the performance of dual-hydrogen-bonding organocatalysts in model reactions. Complexes of 25 dual-hydrogen-bonding organocatalysts with methyl vinyl ketone (MVK) and nitroethylene (NE) were studied, along with the transition states for the corresponding organocatalyzed Diels-Alder cycloaddition of MVK with cyclopentadiene (CPD) and the Friedel-Crafts alkylation of NE with indole. Overall, the results reveal key relationships between catalyst binding energy and catalytic efficacy, and provide quantitative information about the hydrogen bond strengths and transition state lowering ability of a wide range of model catalysts for these two reactions. These data will help design more effective dual-hydrogen-bonding catalysts for the synthesis of complex chiral molecules and natural products.

ACKNOWLEDGMENTS

This research relies on the generous support from the National Science Foundation (Grants CHE-1266022 and CHE-1359175) and the Welch Foundation (Grant A-1775). I would also like to thank the Texas A&M High Performance Research Computing facility for computational resources, and the Texas A&M Undergraduate Research Scholars for their assistance with this thesis.

I would also like to acknowledge those who provided wonderful ideas and entertaining discussions that contributed to this research. Thank you very much to the Wheeler Group, Kimberley Q. Fern, Analise Doney, and, of course, Dr. Daniel A. Singleton.

Finally, I want to extend my sincerest gratitude and heartfelt thanks to my research advisor, Dr. Steven E. Wheeler, for encouraging me to get through “the cloud” despite how often I erred along the way. I would not be where I am without your support, and I am incredibly grateful for the vast opportunities you opened for me. Your excitement about your research and your willingness to help young scientists succeed is truly inspiring. I hope that is something I can take with me when I go… and all three of my Wheeler Group mugs.

CHAPTER I

INTRODUCTION

The demand for high-yield enantioselective reactions drives research in organocatalysis, specifically in small-molecule organocatalysis. Holding notable advantages over biocatalysts and metal-catalysts, small-molecules organocatalysts are generally less expensive and tend to be more stable than their metal-containing counterparts.[1,2] Additionally, small-molecule organocatalysts may be easily modified to mimic natural enzyme catalysis mechanisms.[3] Furthermore, many metal-catalysts are toxic to humans and aquatic species, whereas organocatalysts are usually significantly less harmful to our health and the environment.[4,5]

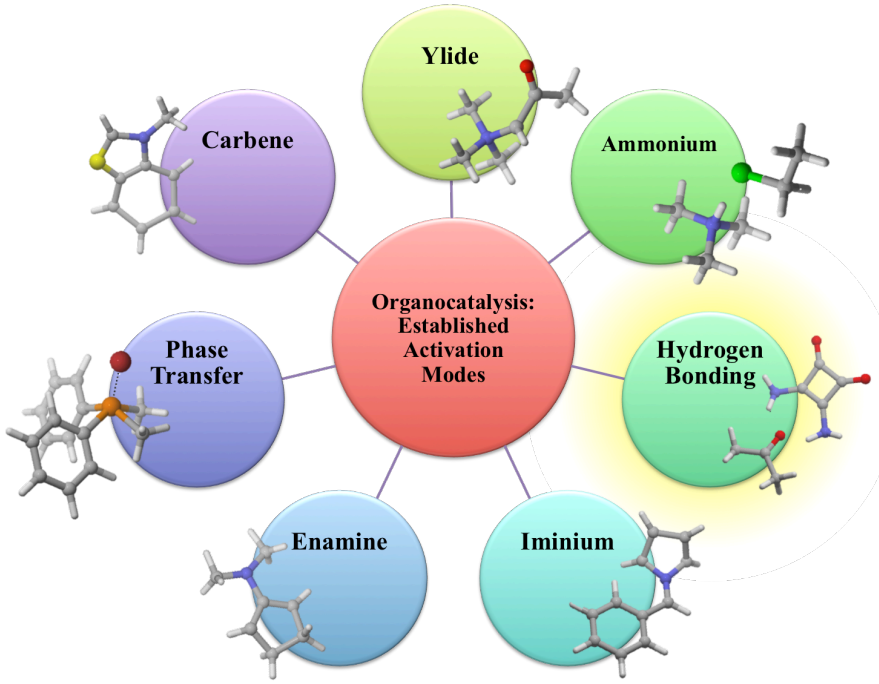

Figure 1. The seven established activation modes of organocatalysts as classified by MacMillan.[2] Hydrogen-bonding organocatalysts form only non-covalent interactions with a substrate.

Like metal catalysts, organocatalysts are very diverse, and have been demarcated into seven classes based on their activation mode, as shown in Figure 1. This research focuses on catalysts that activate reactions by forming hydrogen bonds with one or more of the reactants. Despite relying on weak, non-covalent interactions as activation modes, many hydrogen-bonding catalysts exhibit exceptional catalytic efficacy.[6] Hydrogen-bonding activates many substrates by shifting electron density from the substrate towards the catalyst, rendering them more susceptible to nucleophilic attack. Hydrogen bonding interactions also stabilize the LUMO of many substrates, enhancing their reactivity in many pericyclic reactions. By the same principle, the transition states of hydrogen-bonding catalyzed reactions are stabilized by non-covalent interactions, which leads to lower activation barriers and greater reaction rates.[7,8] Additionally, hydrogen-bonding organocatalysts are active even in highly coordinating solvents.[8] Dual-hydrogen-bond (DHB) donors, a class of hydrogen-bonding catalysts, possess all of these traits in addition to the ability to prohibit substrate rotation about a single hydrogen bond, as illustrated in Figure 2. Since two hydrogen bonds limit the possible geometries of the transition structure (TS), DHB organocatalysts tend to be more regio- and stereo-selective than single-hydrogen-bonding organocatalysts.[8]

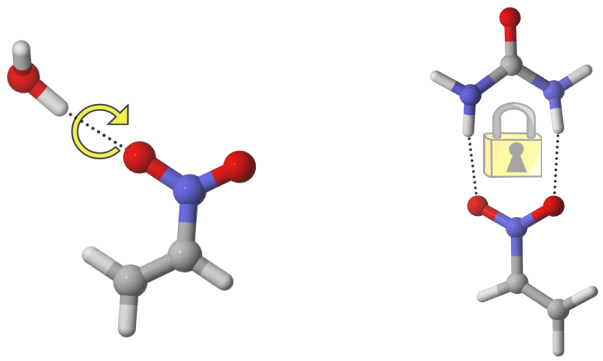

Figure 2. Dual-hydrogen-bonding organocatalysts limit substrate rotation. On the left, the single hydrogen bond between water and NE allows for rotation around a single hydrogen bond, while on the right, urea locks the orientation of NE with two hydrogen bonds.

DHB donors have long been exploited to bind negatively charged species for the purpose of molecular recognition. However, research in hydrogen bond catalysis over the last 15 years has focused primarily on the development of DHB donating groups that activate neutral species in organocatalytic reactions.[8] Currently, it is not well established which DHB donor forms the strongest hydrogen bonds with common neutral DHB acceptors or how hydrogen bond strength translates into catalytic efficacy. Moreover, the strategic design of novel, more effective hydrogen-bonding organocatalysts is only possible if we understand the fundamental interactions governing DHB organocatalysis.

In an effort to elucidate the relationship between hydrogen-bonded complex (HBC) strengths and catalytic activities, Kozlowski and coworkers used UV-Visible spectroscopy (UV-Vis) to measure the absorbance maximum between a chromophore sensor **S**, (λ_S), and the sensor-catalyst HBC, (λ_{HBC}), as outlined in Scheme 1. Then, they experimentally determined the HBC binding constant (K_{eq}). Compared to **S**, the HBCs exhibited absorbance maxima at shorter wavelengths. The blue shift in wavenumbers, that is, ($1/\lambda_{HBC} - 1/\lambda_S$), and the natural log of K_{eq} were strongly correlated.[9] This correlation is not surprising because both terms are linear with respect to energy.

Next, Kozlowski et al. measured the catalyzed reaction rates (k_{rel}) of the Diels-Alder cycloaddition of methyl vinyl ketone (MVK) and cyclopentadiene (CPD) and the Friedel-Crafts alkylation of N-methylindole and nitrostyrene. Like K_{eq}, the natural log of k_{rel} was strongly correlated with the blue shift. From this data, Kozlowski concluded that the blue shift of the

sensor-catalyst HBC is related to the catalyzed rate, and that the activity of a hydrogen-bonding catalyst can be quantified by the strength of the sensor-catalyst HBC.[9]

Scheme 1. Equilibrium of S and DHB Catalyst 1

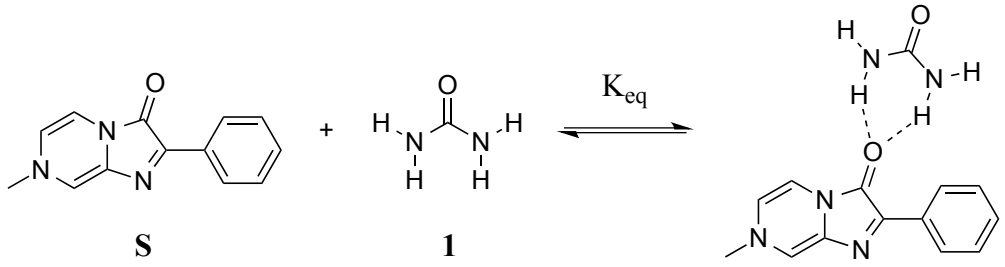

Absorbs in red region
Absorbance wavelength: λ_S

Absorbs in blue region
Absorbance wavelength: λ_{HBC}

However, the final conclusion is based on two assumptions. First, Kozlowski and coworkers assumed that the sensor-catalyst binding constant is proportional to the binding constants of the HBCs with MVK or NE. Similarly, they assumed that the MVK-catalyst HBC binding constant is proportional to k_{rel}. In other words, as is commonly done in the literature, they implicitly assumed that the strength of the hydrogen bonds between the substrate **S** and a catalyst is proportional to the catalyst's activity in the Diels-Alder and Friedel-Crafts reactions.

Herein, we present a comprehensive study of dual-hydrogen-bonding organocatalysts to test the validity of Kozlowski's assumptions, to quantify the catalytic activity of 25 catalysts (Scheme 2) in the Diels-Alder cycloaddition of CPD and MVK and the Friedel-Crafts alkylation of Nitroethylene (NE) and indole (Scheme 3), and to derive the relationship between HBC strength and the catalytic activity. To accomplish this, energetic and structural properties of substrate-

DHB donor complexes and DHB catalyzed transition states were computed with density functional theory (DFT), a modern computational quantum mechanical method. The free energies of the key intermediates defined in Figure 3 provide insight into the fundamental interactions regulating DHB organocatalysis. Additionally, ΔG_{bind} and $\Delta G^{\ddagger}$ represent the difference in free energy between the HBC and the reactants, and the difference in free energy between the TS and the reactants, respectively.

Scheme 2. Dual-Hydrogen-Bonding Organocatalysts Studied

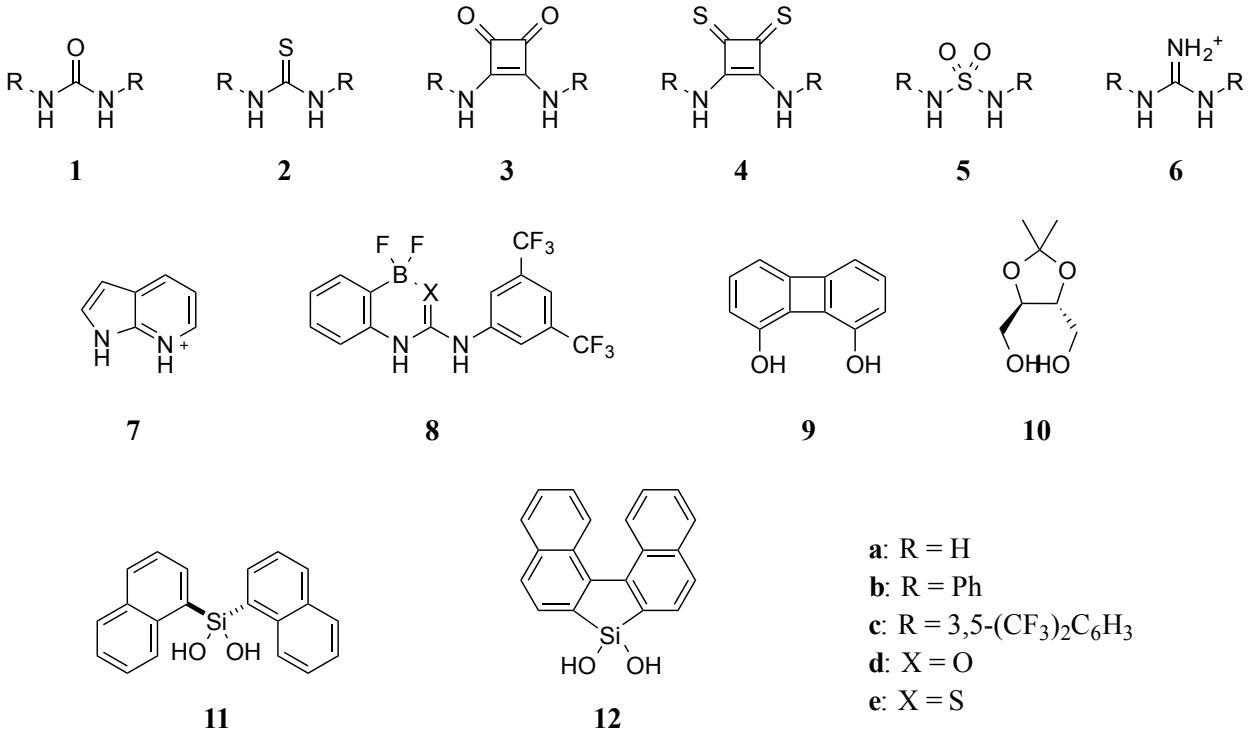

In contrast with Kozlowski's initial assumption, a poor correlation was found between the sensor-HBC strengths and the substrate-HBC strengths. Therefore, the blue shift in the sensor-catalyst HBC cannot be used as a reliable predictor of catalytic activity. In order to understand the origin of DHB organocatalysis, the strongest DHB donors and most effective catalysts were

determined for MVK and NE, and the relationship between HBC strength and transition state stabilization was investigated. A correlation between HBC strength and catalytic activity was found for Diels Alder cycloadditions, but not Friedel Crafts alkylations. Furthermore, the optimal catalyst was not the same across both reactions, highlighting the challenge of developing broad-acting hydrogen-bonding catalysts. Because the two reactions differed substantially in terms of substrate binding modes, HBC strengths, and rate enhancements, the results conclusively show that no single catalyst is optimal for all organic substrates or transformations. However, structural motifs were identified that could qualitatively predict the activity of DHB organocatalysts, suggesting a route to the design of more effective catalysts.

Scheme 3. Model Diels-Alder and Friedel-Crafts Reactions Catalyzed by DHB Donors

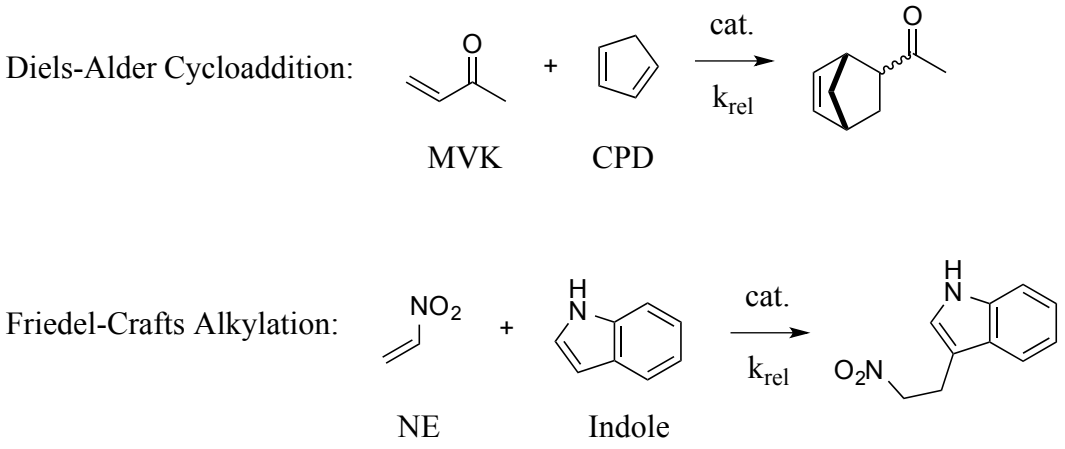

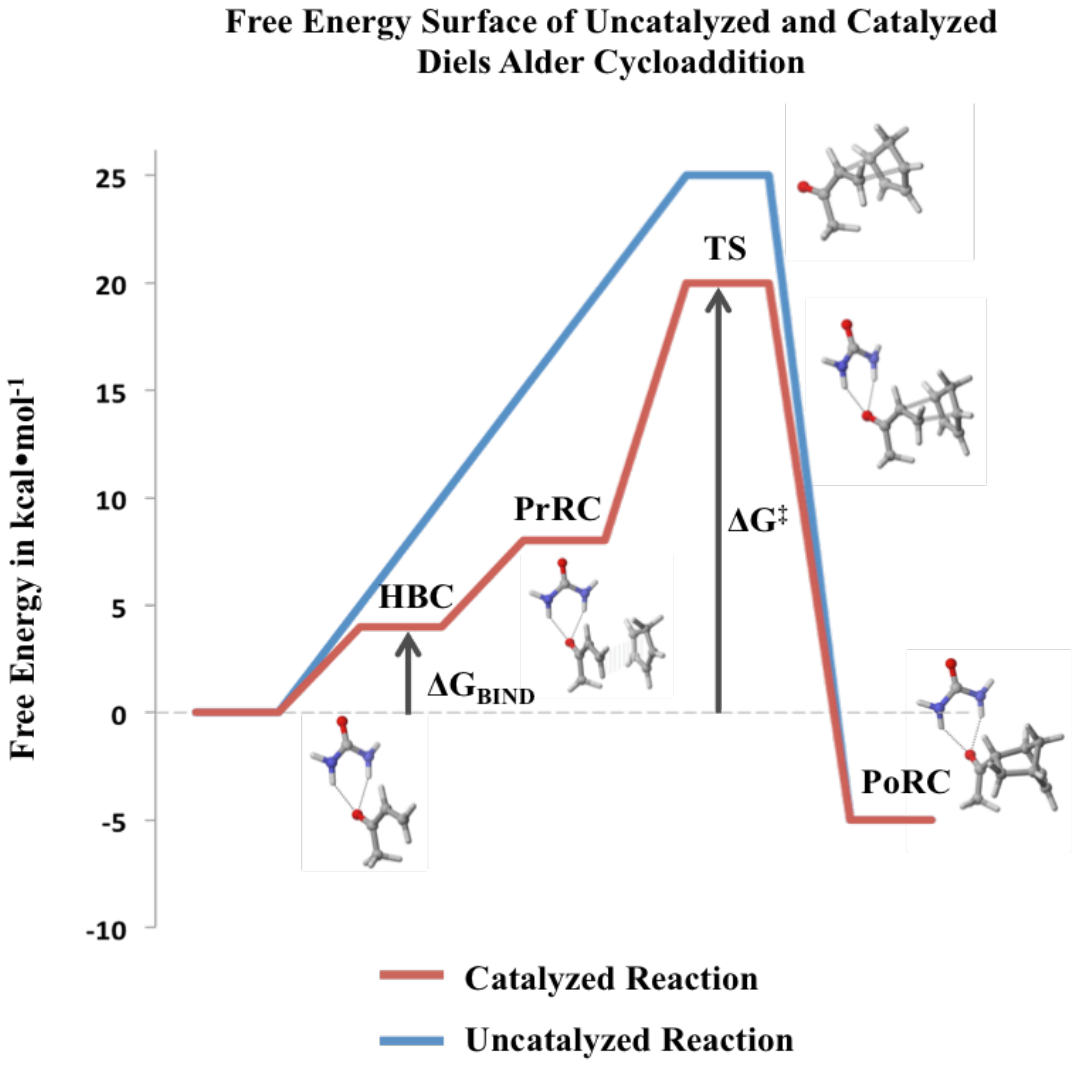

Figure 3. Free energy profile of the uncatalyzed (blue) and urea-catalyzed (red) Diels-Alder cycloaddition of MVK and CPD. Key structures include the hydrogen-bonded complex (HBC), pre-reaction complex (PrRC), transition structure (TS), and post-reaction complex (PoRC). The HBC is the complex between the hydrogen-bonded substrate and catalyst, while the PrRC is a non-bonded complex between the substrate and catalyst as well as cyclopentadiene. The TS is the geometry of the transition state, and the PoRC is the hydrogen-bonded complex of the product with the catalyst. The strength of the HBC is represented by ΔG_{bind}, and the activation energy of the reaction is given by $\Delta G^{\ddagger}$.

CHAPTER II

METHODS

Geometry optimizations were performed at the PCM-M06-2X/6-31+G(d) level of theory, with dichloromethane as a model solvent, followed by single-point energy computations at the ωB97-XD/def2-TZVP level of theory.[10,11] All structures presented are fully optimized, and are characterized by either zero imaginary vibrational frequencies (energy minima) or a single imaginary frequency (transition states). In preliminary work, use of a (75,302) integration grid led to persistent problems locating true stationary points for these complexes at the M06-2X/6-31+G(d) level of theory; thus, we employed an ultrafine integration grid with 99 radial and 590 angular points.

For each hydrogen bond donor-acceptor pair, we systematically searched to identify all low-lying energy minima for DHB donor-substrate complexes and transition states in accordance with the Curtin-Hammett principle.[12] Quantitative comparisons of the binding complexes (HBC), and transition states (TS) are based on the free energy at 298.150 K in kcal•mol^{-1}. The difference in free energy between the infinitely separated reactants and the HBC is given by ΔG_{bind}, while $\Delta G^{\ddagger}$ represents the difference between the reactants and the TS (see Figure 3).

Molecular structure figures were produced using CYLView.[13] NCI plots, which show red, blue, and green areas that represent repulsive, attractive, and dispersion interactions, respectively, were created using Jmol.[14-16]

CHAPTER III

RESULTS

Benchmarking computations

DHB organocatalysts are challenging to study with DFT since popular functionals, such as B3LYP, often underestimate reaction barriers and hydrogen bonding interaction energies.[10] However, computational studies can give insight into structural properties that are difficult to observe experimentally. Additionally, the efficacy of novel catalysts, such as **8e**, can be determined before they are ever synthesized.[17]

To demonstrate the reliability of using computational chemistry to study the complex interactions involved in DHB organocatalysis, computed HBC binding energies were compared to experimental measurements from First, the DHB organocatalysts in Scheme 2 for which experimental K_{eq} data are available from Kozlowski et al.[9] were selected. Seven catalysts, **1c**, **2b**, **2c**, **5c**, **6b**, **8d**, and **11**, fit these criteria. Then, the HBC geometries between **S** and the selected catalysts were optimized at the M06-2X/6-31+G(d) level of theory, and the theoretical binding energies, ΔG_{bind}, were computed at the ωB97-XD/def2-TZVP level of theory. To model the experimental conditions as accurately as possible, computations were performed in a dichloromethane PCM solvent model.[9] The experimental values for K_{eq} were converted to free energies using equation 1

$$\Delta G_{bind,Exp} = -R \cdot T \cdot \ln K_{eq} \qquad \text{Eq. 1.}$$

where R = 1.986×10^{-3} kcal•$K^{-1}$$mol^{-1}$ and T is the temperature (298.15 K). The experimental and theoretical HBC free energies are presented in Table 1.

Table 1. Experimental and Theoretical Data for HBC Complexes of Selected Catalysts with Sensor S, MVK, and NE.

Catalyst	Experimental K_{eq} (M^{-1})	Experimental $\Delta G_{bind,S}$ (kcal•mol^{-1})	Theoretical $\Delta G_{bind,S}$ (kcal•mol^{-1})	$\Delta G_{bind,MVK}$ (kcal•mol^{-1})	$\Delta G_{bind,NE}$ (kcal•mol^{-1})
1c	9.38×10^3	-5.42	-3.78	3.01	3.88
2b	1.67×10^1	-1.67	-0.40	0.02	1.38
2c	1.77×10^3	-4.43	-4.47	1.59	4.02
5c	1.04×10^3	-4.11	-2.88	0.21	2.44
6b	1.84×10^4	-5.81	-5.18	0.26	1.34
8d	2.65×10^4	-6.03	-5.72	0.39	2.01
11	7.88×10^1	-2.59	-2.25	2.33	6.07

As shown in Table 1, computations predict that **S** will form the strongest HBCs with catalyst **8d** and the weakest HBCs with catalyst **2b**, which qualitatively agrees with experiment. Moreover, Figure 4 shows that the theoretical and experimental values for ΔG_{bind} are highly correlated (R^2 = 0.89). Thus, changes in free energy can be quantified with considerable accuracy. While a correlation constant of R^2=1 is ideal, the effects of the error intrinsic to DFT computations and of the indeterminate error propagated through the experimental procedures are significant with respect to the small data set. Since the error is inherent to both systems, the standard deviation would decrease if more HBC strengths were compared. Therefore, results from the benchmark

confirm that quantum computational chemistry, more specifically the ωB97-XD density functional, can quantitatively describe DHB systems.

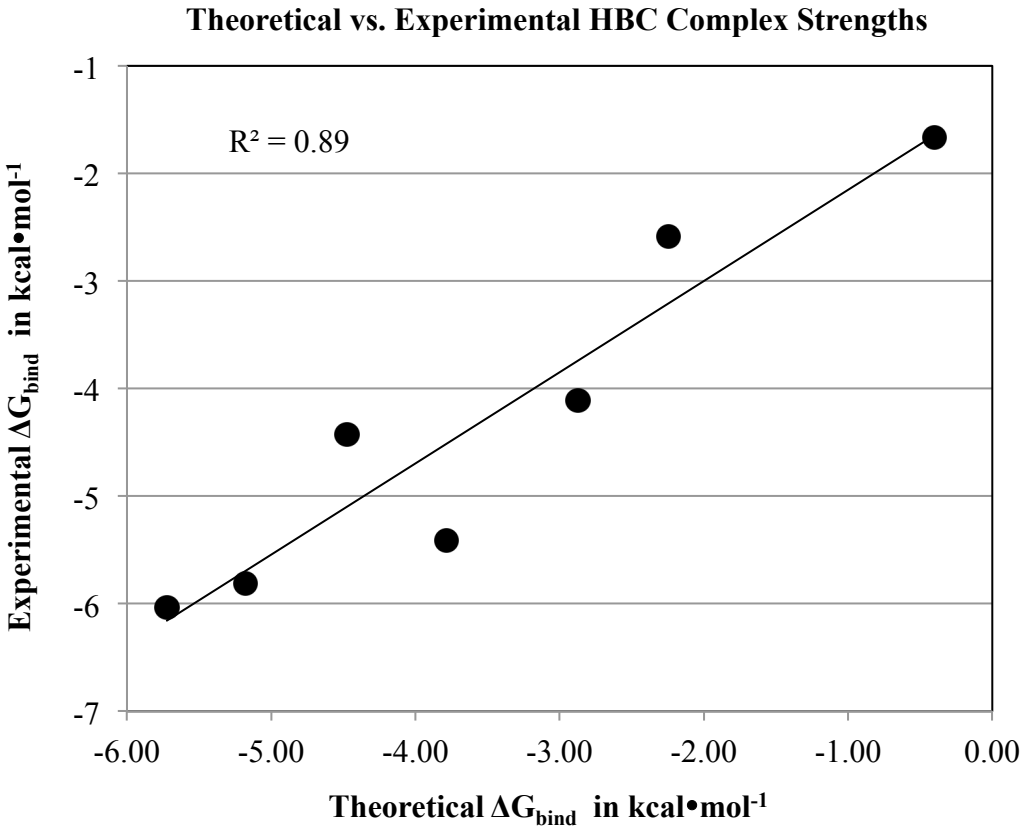

Figure 4. Experimental and computed binding free energy for HBC complexes of **1c**, **2b**, **2c**, **5c**, **6b**, **8d**, and **11** with sensor **S**.

Limitations of chromophores

Since the chosen level of theory is reliably reproduces HBC binding free energies, computational data can be used to directly assess the assumption of Kozlowski et al. that the binding free energy for **S** with a given catalyst is proportional to the binding free energy for MVK or NE with the same catalyst. MVK and NE HBC binding free energies with **1c**, **2b**, **2c**, **5c**, **6b**, **8d**, and **11**

were computed and are reported in Table 1. In Figure 5, computed $\Delta G_{bind,MVK}$ (blue) and $\Delta G_{bind,NE}$ (red) are plotted against the experimentally measured $\Delta G_{bind,S}$,.

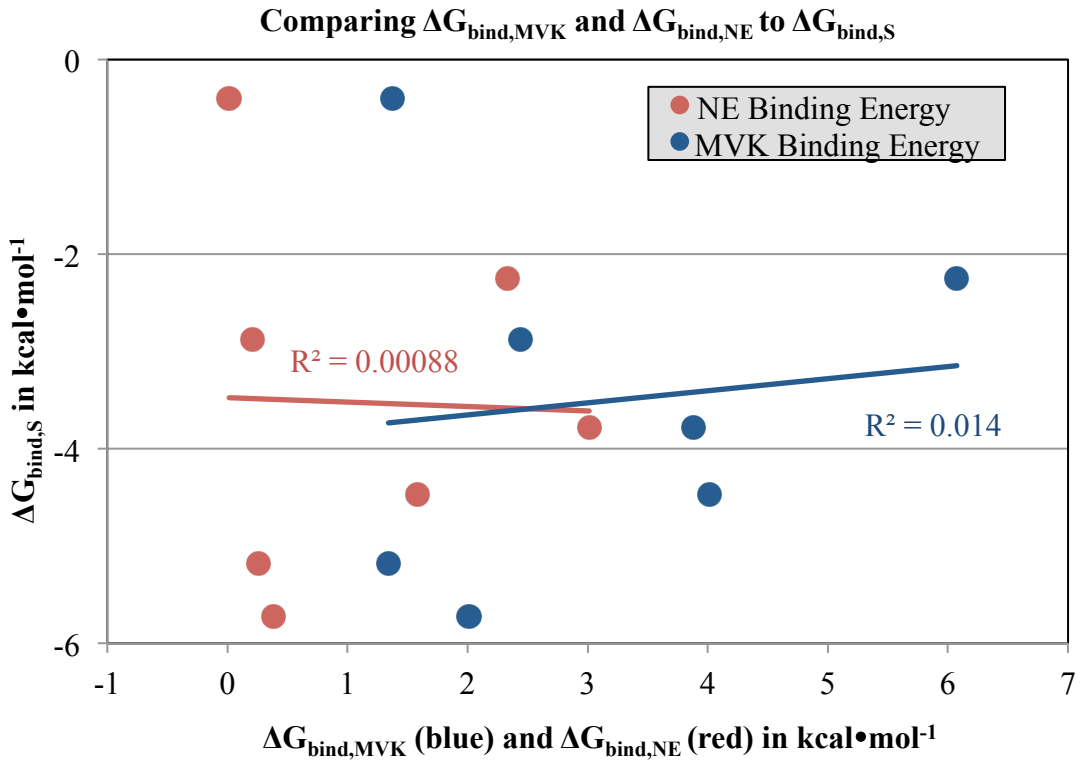

Figure 5. $\Delta G_{bind,MVK}$ (blue) and $\Delta G_{bind,NE}$ (red) plotted against $\Delta G_{bind,S}$.

As shown in Table 1, the formation of the MVK- and NE-DHB complexs is endergonic, whereas all S-DHB complexes are lower in free energy than the separated components. More importantly, neither $\Delta G_{bind,MVK}$ nor $\Delta G_{bind,NE}$ are correlated with $\Delta G_{bind,S}$. Therefore, the S-HBC binding free energies do not provide even qualitative predictions of MVK or NE binding free energies. To determine the origin of the differences, the optimized **S**-HBC geometries were analyzed and compared to the MVK- and NE-HBC geometries.

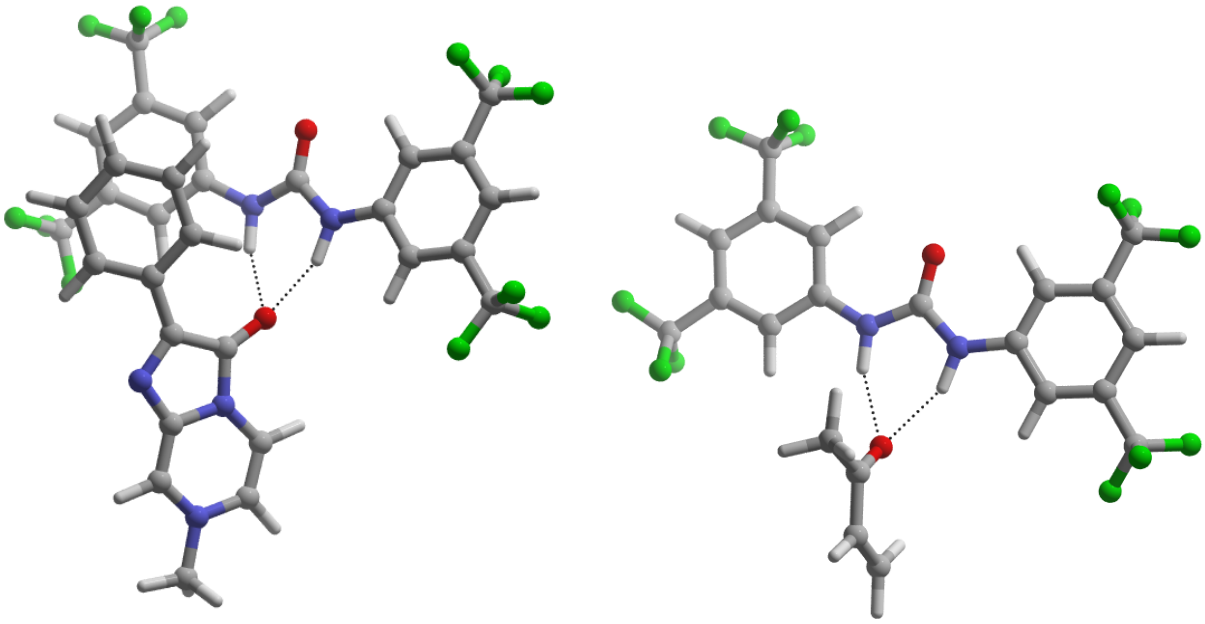

Figure 6. HBC of **1c** with the sensor **S** (left) and with MVK (right).

As shown in Figure 6, both **S** and MVK are accepting two hydrogen bonds from the acidic protons of the thiourea. However, the phenyl ring of **S** is engaged in a π-stacking interaction with the substituted aryl substituent on **1c**. Aryl substituents provide a powerful means of tuning the strength of π-stacking interactions, albeit inadvertantly in this case.[18-22] In the work of Kozlowski et al., **S** was chosen as an ideal sensor for DHB complex formation because it can accept multiple hydrogen bonds and is a chromophore, meaning that it is active in the UV-Vis region. Therefore, **S** has a small HOMO-LUMO gap, is highly conjugated, and small changes in its orbitals, such as those that occur when HBCs are formed, can be measured with UV-Vis. However, the extensive conjugation needed for an organic molecule to be UV-Vis active renders it susceptible to π-stacking interactions with other aryl rings. Because non-covalent aryl-aryl interactions are favored enthalpically, the net free energy of the **S**-**1c** system decreases, and the HBC is favored at equilibrium. In most cases (see Figure 7), MVK and NE cannot form π-

complexes with the DHB catalysts. Consequently, the free energy of the MVK- or NE-HBC increases due to the entropic cost of bringing two molecules together. Thus, MVK- and NE-HBCs are disfavored slightly at equilibrium.

While π-stacking is beneficial for many catalytic applications and in the context of drug design,[23-26] these non-covalent interactions complicate the use of **S**-HBC binding energies as predictors of MVK- or NE-HBC binding energies, since the the HBC complexes of these smaller substrates are not stabilized by aryl-aryl interactions. The result is that the wavelength shift measured in the recent work of Kozlowski et al. cannot quantify the hydrogen bonding strength of DHB organocatalysts with either substrate, or the activity of the catalysts in Diels-Alder cycloadditions and Friedel-Crafts alkylations.

Dual hydrogen bonded complexes

Having explored the subset of catalysts for which there was experimental HBC binding free energies, we next turn to the HBCs of MVK and NE with the full set of model hydrogen bonding catalysts in Scheme 2. For each substrate and catalyst pair, several HBCs were computed, and the lowest binding free energy is reported in Appendix A. The MVK-HBC binding free energies spanned from -2.24 to 5.85 kcal•mol^{-1}. Catalysts **3c** (ΔG_{bind} = -2.24 kcal•mol^{-1}) and **9** (ΔG_{bind} = -0.87 kcal•mol^{-1}) formed the strongest HBCs with MVK, which are shown in Figure 7. In both complexes, two hydrogen bonds are formed between the oxygen atom in MVK and the acidic protons in **3c** or **9**. However, the binding mode, or orientation of the substrate with respect to the catalyst, differs markedly between the complexes. In the complex with **3c**, MVK is twisted at an angle of 37.8° with respect to the plane of **3c**, but MVK is almost perpendicular to **9** at 88.4°.

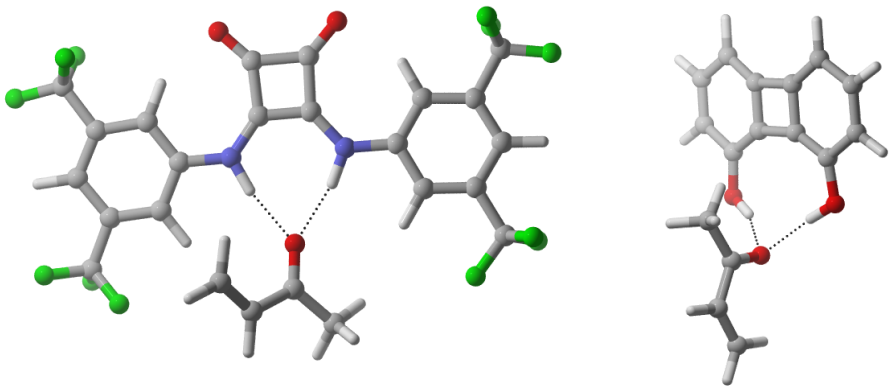

Figure 7. HBCs of MVK with **3c** (left) and **9** (right).

In contrast, catalysts **5a** (ΔG_{bind} = 5.85 kcal•mol^{-1}) and **12** (ΔG_{bind} = 5.66 kcal•mol^{-1}) formed the least favorable HBCs with MVK and are shown in Figure 8. Both complexes have two hydrogen bonds between the catalyst and MVK, and MVK adopts a twisted binding mode (32.2°) in the HBC with **12**. The **5a**-MVK HBC has a unique binding mode characteristic of the sulfamide catalysts **5a**, **5b**, and **5c**, in which the hydrogen bonds are far from the molecular plane of the MVK. This can be explained by the presence of attractive non-covalent interactions between the one of the sulfamide oxygens and the carbon of the carbonyl of MVK, as shown in the NCI plot in Figure 9. This interaction arises from the interaction between the nucleophilic sulfamide oxygen and the electrophilic carbonyl carbon.

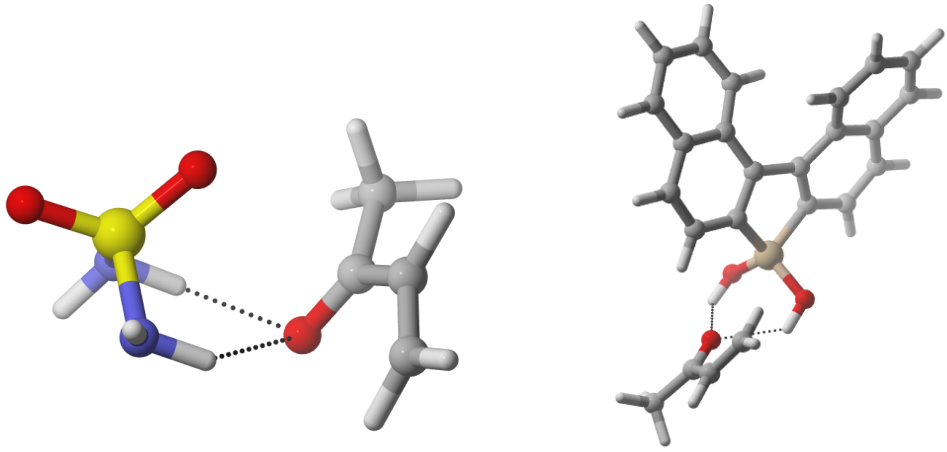

Figure 8. HBCs of MVK with **5a** (left) and **12** (right).

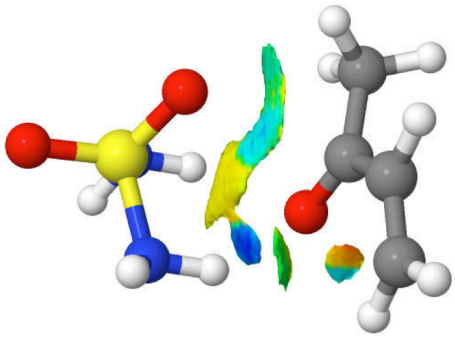

Figure 9. NCI plot showing the attractive interaction between the carbonyl carbon and sulfamide oxygen in the **5a**-MVK HBC.

However, MVK does not always interact with both acidic protons of the catalysts. Shown on the left in Figure 10, only one hydrogen bond is formed between catalyst **11** and MVK. Rather than forming two hydrogen bonds, MVK's C=C bond interacts with the aromatic ring. Although this conformation results in a relatively weakly bound HBC (ΔG_{bind} = 2.33 kcal•mol^{-1}), the alternative binding mode with two hydrogen bonds (Figure 10, right) is 2.24 kcal•mol^{-1} higher in free energy. In this instance, the π-stacking interaction between MVK and the aromatic

component of the catalyst is more favorable than forming a second hydrogen bond. This is due to the repulsion of the protons highlighted in green in Figure 10. In Figure 10, the H-H distance of the left HBC is 3.08 Å, while the same distance for the right HBC is 3.05 Å. Therefore, forming two hydrogen bonds requires catalyst **11** to distort in such a way that increases the strain in the catalyst.

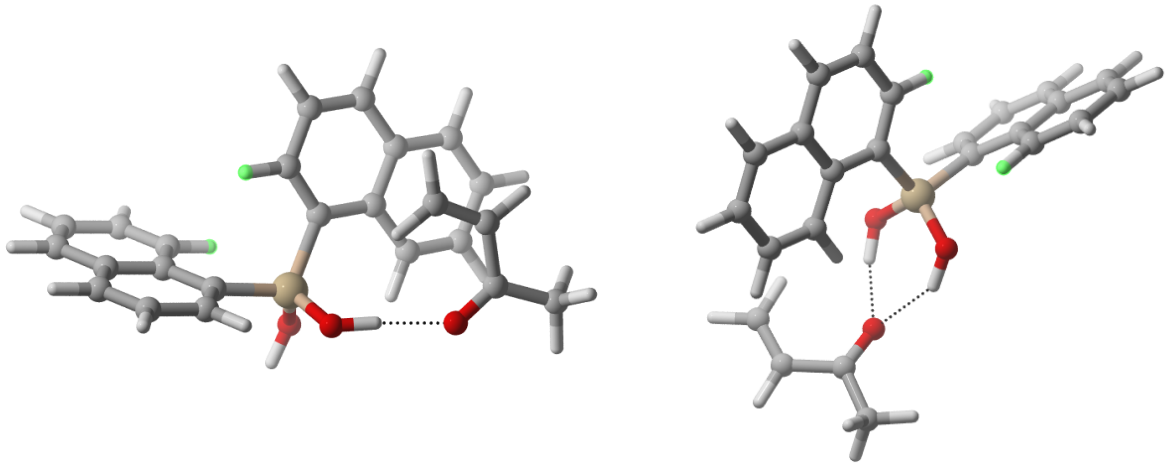

Figure 10. The most stable HBC between MVK and **11** (left) has one H-bond, while a less stable complex (right) has two H-bonds. The distance between the protons highlighted in green in the left structure is 3.08 Å, while the same distance in the right structure is 3.05 Å.

The binding energies for NE-HBCs spanned from 1.22 to 5.85 kcal•mol^{-1}, and **3c** formed the strongest HBC with NE, as observed for MVK. However, while **9** formed the second strongest HBC with MVK, it formed the fourth weakest HBC with NE at 5.53 kcal•mol^{-1}. Catalyst **12** formed the weakest NE-HBC, with ΔG_{bind} = 5.85 kcal•mol^{-1}. Structures of the NE-HBCs with catalysts **3c** and **12** are shown in Figure 11.

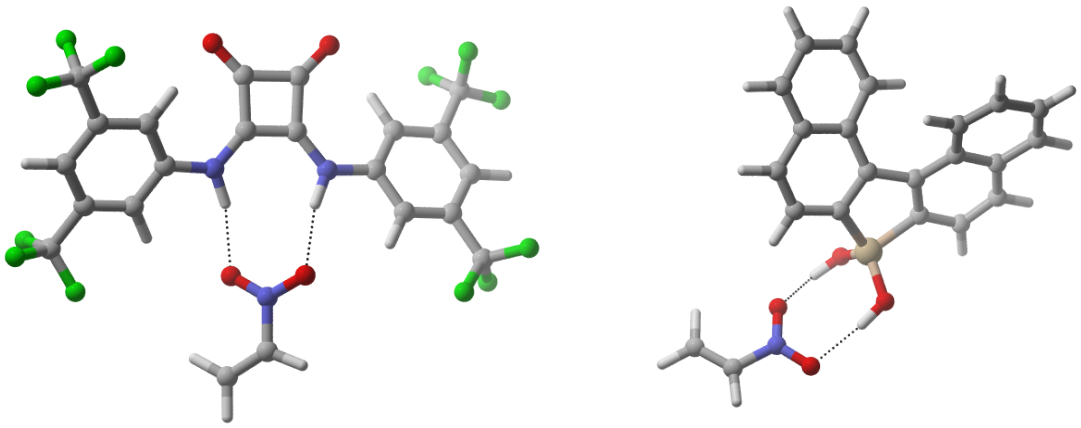

Figure 11. Geometries of NE-HBCs with catalysts **3c** (left) and **12** (right).

As seen with MVK, there are multiple possible binding modes for NE-HBCs, as shown in Figure 12. For all of the lowest energy NE-HBCs, NE is in the same plane as, or is slightly twisted with respect to, the plane of the catalysts' H-bonds, and each oxygen in the nitro group forms one hydrogen bond with the catalyst. However, less favorable optimized structures were found that showed another binding mode where one oxygen formed two hydrogen bonds, similar to a MVK binding motif. A third, "saddle" binding mode has been proposed in the literature in which each oxygen of the nitro group interacts with both catalyst protons. However, no optimized structures were identified exhibiting this proposed binding mode.

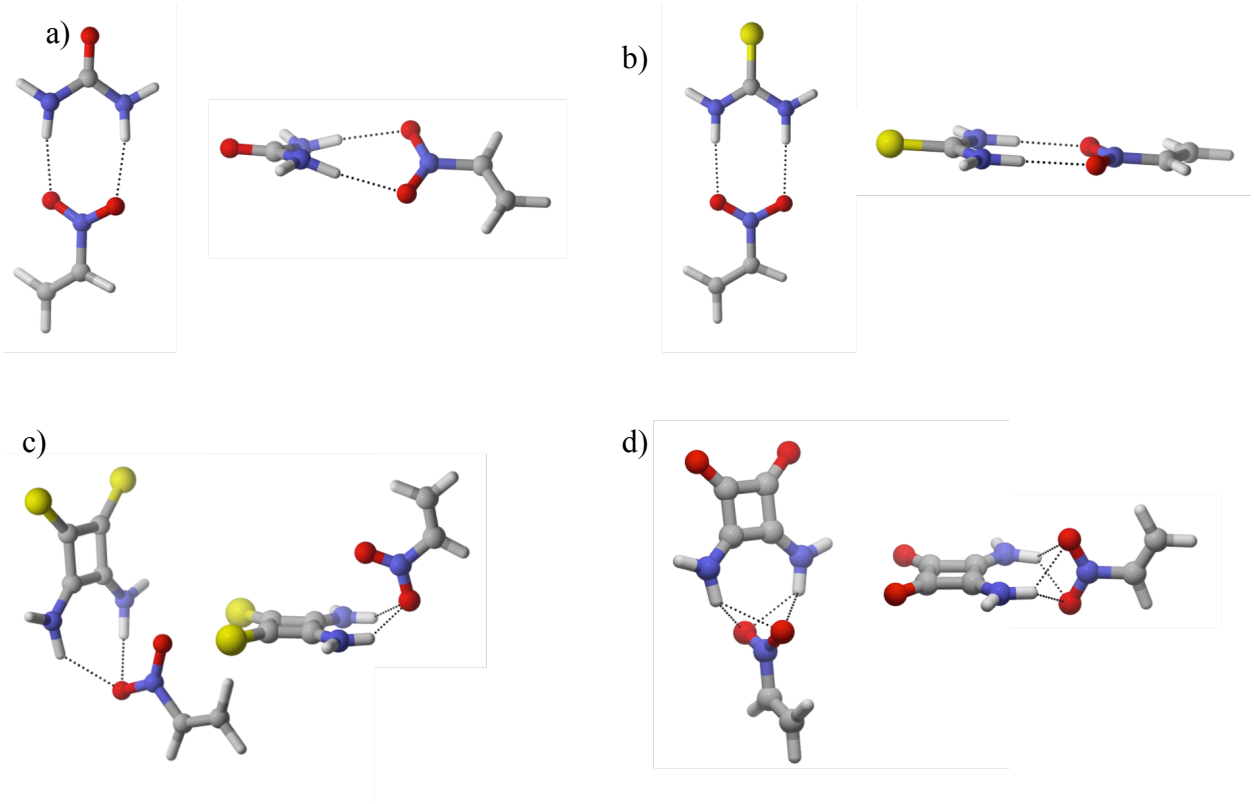

Figure 12. NE-HBCs exhibiting a (a) twisted binding mode, (b) planar binding mode, (c) "1O-2H" binding mode, and (d) "saddle" binding mode with catalysts **1a**, **2a**, **4a**, and **3a**, respectively. The structures in (a), (b), and (c) are fully optimized, while that in (d) is not.

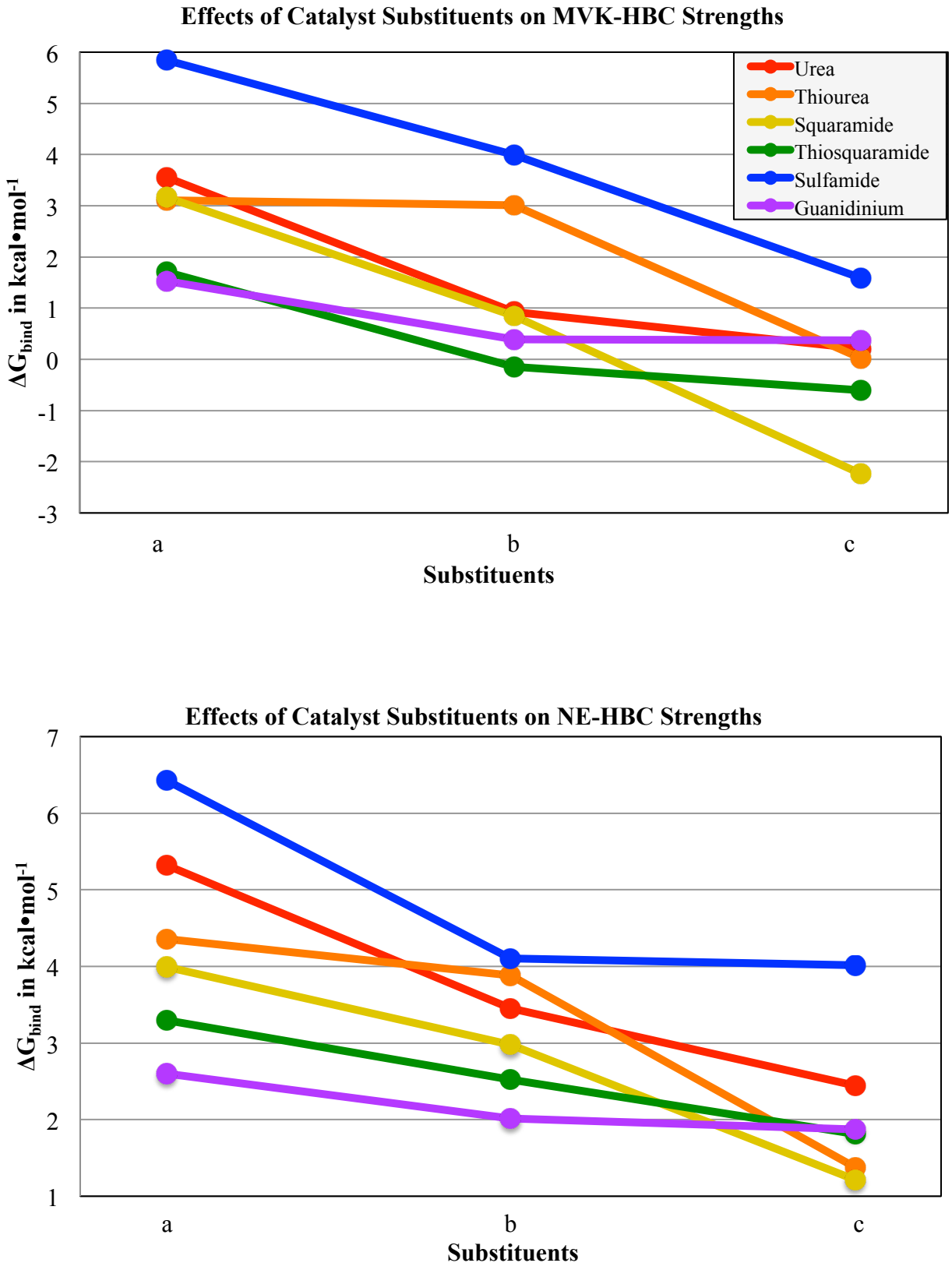

Figure 13. The effects of substituents a, b, and c on HBC strengths.

To explore how substituents affect HBC strength, HBC binding free energies for MVK and NE were plotted against the substituent for catalyst groups **1**-**6** in Figure 13. The downward trend in binding energy versus substituents **a**, **b**, and **c** shows that adding aryl substituents and electron withdrawing groups increases the HBC strength. Schreiner and coworkers suggest that 3,5-bis(trifluoromethyl)phenyl substituents increase the HBC strength because there is a dispersion interaction between the ortho-hydrogen on the substituent and the substrate, MVK.[27] The NCI plot of the **3c**-MVK HBC (ΔG_{bind} = -2.24 kcal•mol^{-1}) shown in Figure 14 supports Schreiner's hypothesis, as the green areas between **3c**'s ortho-hydrogens and MVK are suggestive of weak intermolecular interactions. Therefore, the 3,5-bis(trifluoromethyl)phenyl substituent has an advantage over unsubstituted thiourea. However, the NCI plot for the **3b**-MVK HBC (ΔG_{bind} = 0.84 kcal•mol^{-1}), in which there are no substituents on the aryl group, shows similar non-covalent interactions between the ortho-hydrogens and MVK; moreover, the green surface has a larger volume than that in **3c**'s NCI plot, suggesting more extensive dispersion interactions in this case. Thus, Schreiner's hypothesis that 3,5-bis(trifluoromethyl)phenyl increases HBC strength because of dispersion interactions between the ortho-hydrogens and the substrate does not explain why **3c** forms stronger HBCs than **3b**.

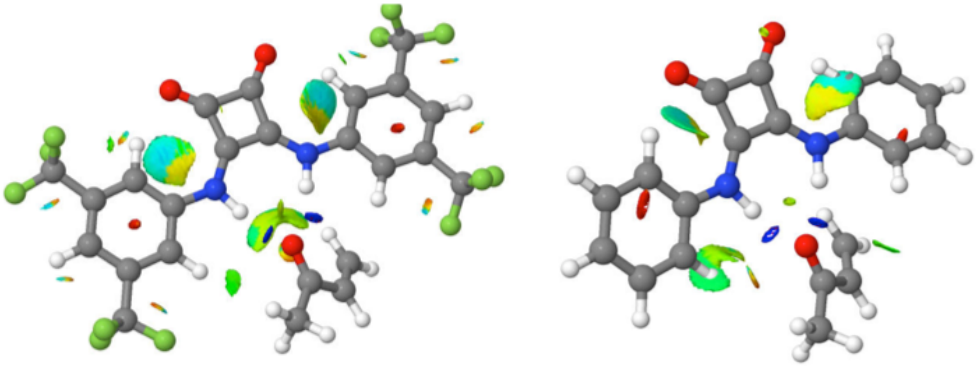

Figure 14. NCI plots for the HBCs between MVK and **3c** (left) or **3b** (right).

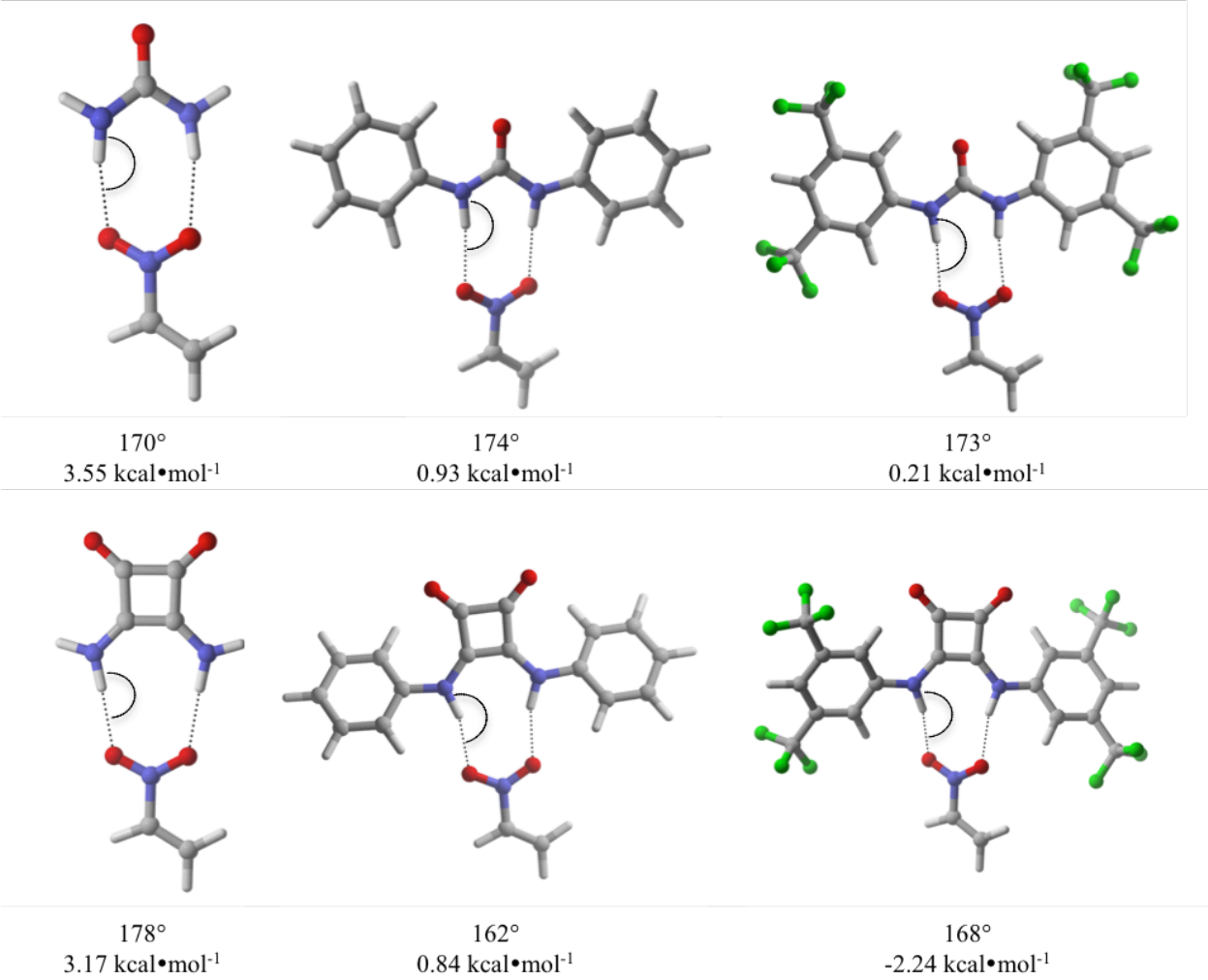

Figure 15. MVK-HBC binding energies and N-H•••O angles for catalysts **1a**, **1b**, and **1c** in the top row, and for catalysts **2a**, **2b**, and **2c** in the bottom row. There is no apparent relationship between the angle and HBC binding energy.

For each substituent, the sulfamide catalysts, **5a**, **5b**, and **5c**, form weaker HBCs with MVK and NE than with any other catalyst with the same substituent. Additionally, the squaramide HBCs are always stronger than analogous urea HBCs; this trend also holds for the relationship between thiosquaramide and thiourea HBCs. In earlier publications, Lu and Wheeler concluded that square shaped catalysts form stronger HBCs than urea-derived analogs because the wider distance between the square catalysts' acidic protons allows the hydrogen bonds to be closer to the ideal 180 degrees.[28,29] N-H•••O angles and binding energies for urea and squaramide

catalysts are shown in Figure 15. While this previously noted relationship between N-H•••O angles and the HBC strength holds for the unsubstituted catalysts (**1a**, **2a**, **3a**, and **4a)**, data for the substituted analogs do not show this relationship. In fact, catalyst **3c** forms the strongest HBCs with MVK and NE, while its N-H•••O angles are farther from ideal than those for the unsubstituted **3a**.

Finally, comparing MVK- and NE-HBC binding free energies, as shown in Figure 16, the correlation constant is 0.58. Qualitatively, DHB catalysts affect MVK- and NE-HBC strengths equivalently, which a few notable outliers. However, a quantitative trend that predicts NE-HBC strengths based on MVK-HBC strengths cannot be made.

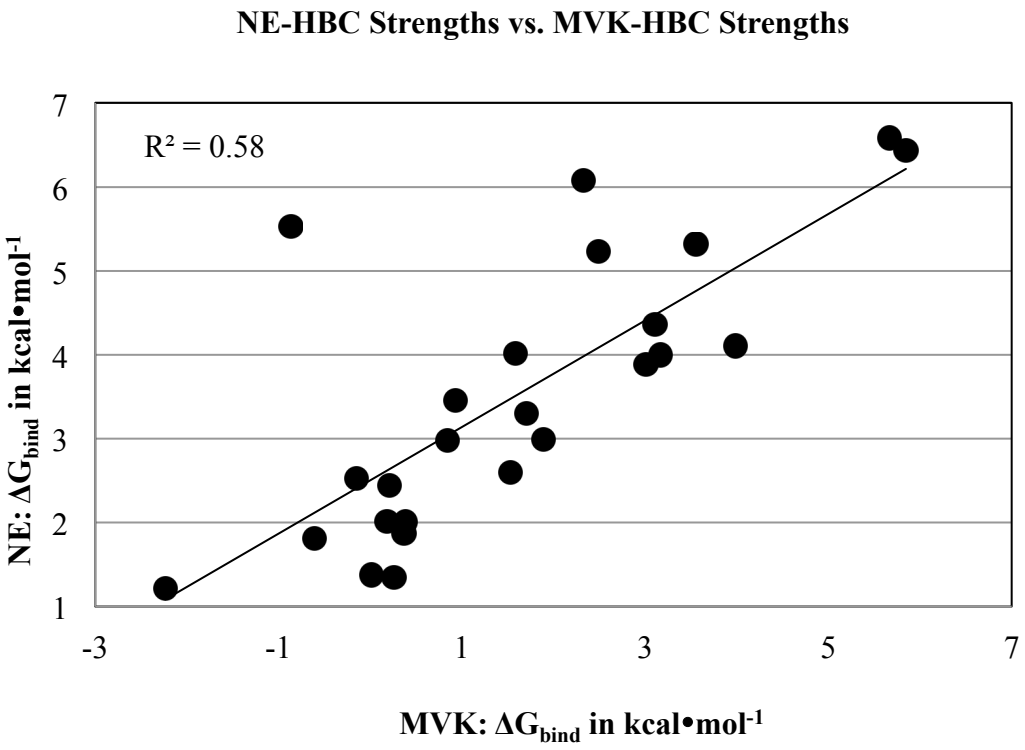

Figure 16. Comparison of NE-HBC strengths and MVK-HBC strengths.

Transition states

Next, we quantify the ability of these 25 model catalysts to stabilize transition states for the Diels-Alder cycloaddition of MVK and CPD and the Friedel-Crafts alkylation of NE and indole. Computed activation barriers are reported in Appendix A. Since the Diels-Alder cycloaddition has a one-step, pericyclic mechanism, the cycloaddition of CPD and MVK is the rate-limiting step. Although the reaction is pericyclic, the formation of the C-C bonds is asynchronous. At the TS, the C-C bond forming between MVK's β-carbon and CPD is longer than that between MVK's α-carbon and CPD. There are four possible uncatalyzed transition states for this reactions, because MVK can be in an s-*cis* or s-*trans* configuration while the reactants can come together to form the *endo* or *exo* products (see Figure 17).

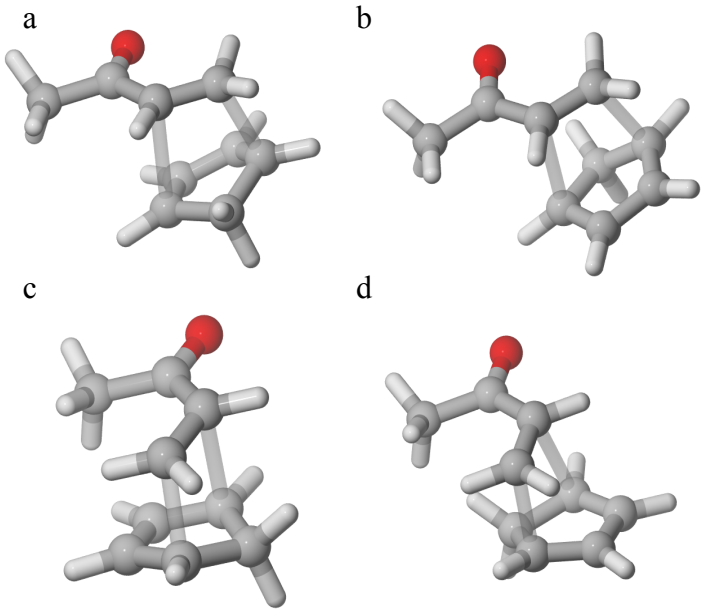

Figure 17. (a) s-*cis endo*, (b) s-*cis exo*, (c) s-*trans endo*, and (d) s-*trans exo* TSs for the Diels-Alder cycloaddition of MVK and CPD.

Of the four transition states, the s-*cis endo* TS is always favored in the case of the catalyzed reactions. The uncatalyzed s-*cis endo* TS activation barrier is 28.76 kcal•mol^{-1}, while the

catalyzed s-*cis endo* barriers range from 20.16 to 31.06 kcal•mol^{-1}. **9** provides the greatest transition state stabilization , and is predicted to increasing the rate of the reaction by a factor of 10^6. In contrast, **5a** is not predicted to accelerate this reaction, because the catalyzed reaction is predicted to be1.7 times slower than the uncatalyzed reaction. TSs for **9** and **5a** are shown in Figure 18.

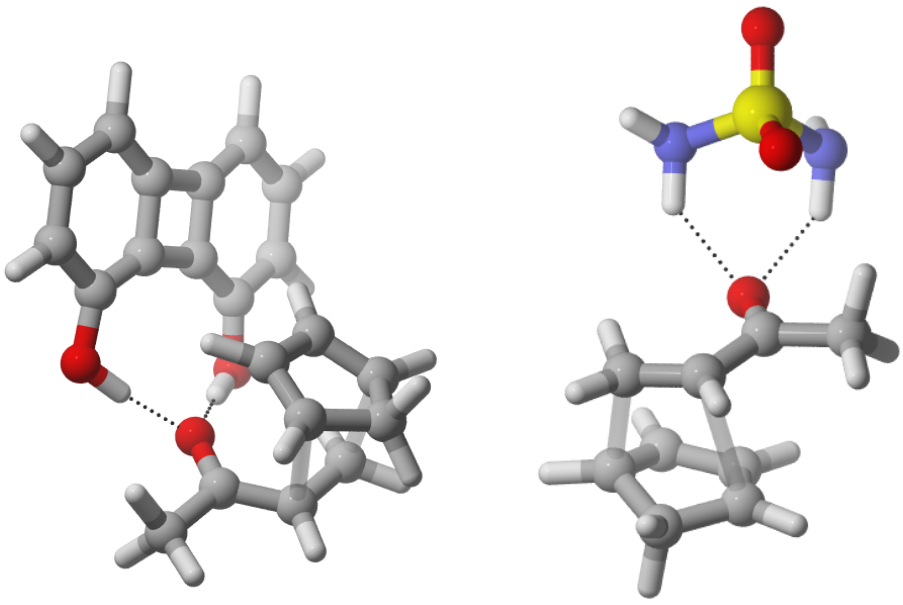

Figure 18. Transition states for the most effective catalyst (**9**, left) and the least effective catalyst (**5a**, right) for the Diels-Alder reaction.

Unlike the Diels-Alder cycloaddition, the Friedel-Crafts alkylation is a multi-step reaction. The addition of NE to indole is the rate-limiting step, and four possible transition states were identified (see Figure 19). The relative orientation in Figure 19a was favored for all of the catalysts.

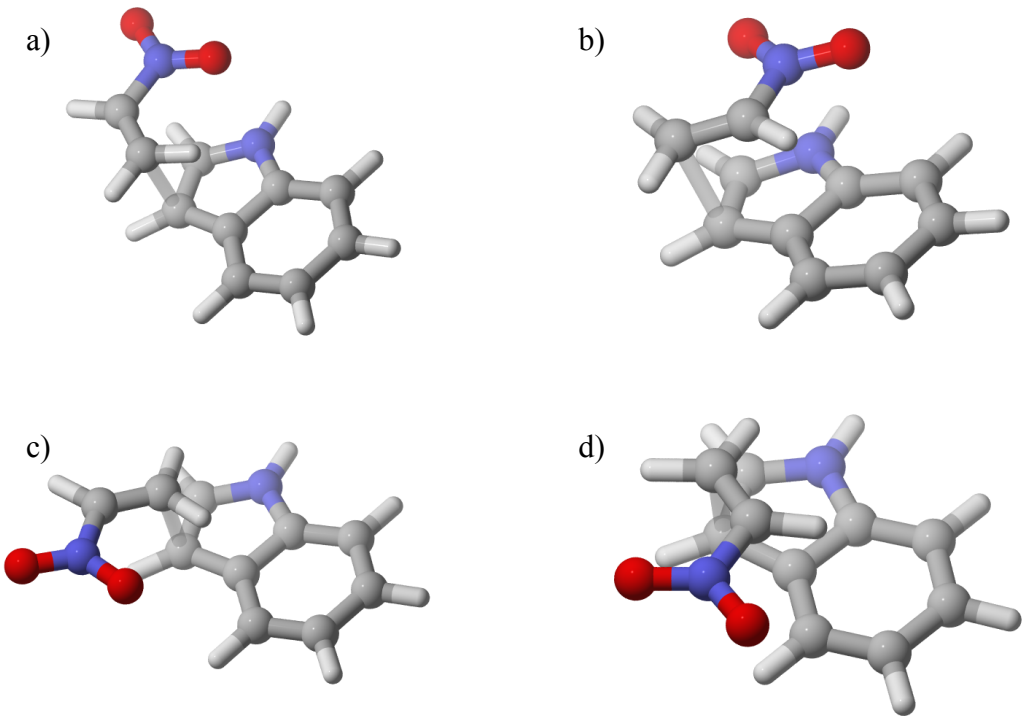

Figure 19. Four TSs for the Friedel-Crafts alkylation of NE and indole. The conformation shown in (a) is predicted to be favored for every TS.

The uncatalyzed activation barrier for the Friedel-Crafts reaction is 28.01 kcal•mol^{-1}, and the most effective catalyst, **3c**, lowered the activation barrier to 18.59 kcal•mol^{-1}. Therefore, the reaction rate is predicted to increase by 10^7 ith **3c**. In opposition, the least efficacious catalyst, **3a**, would not affect the reaction rate, as the catalyst increases the activation energy by 0.47 kcal•mol^{-1}. The TSs for **3a** and **3c** are shown in Figure 20.

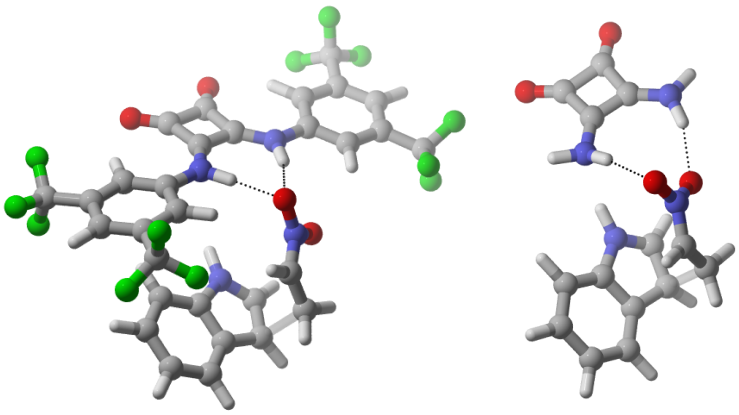

Figure 20. Transition states for the most effective catalyst (**3c**, left) and the least effective catalyst (**3a**, right) for the Friedel-Crafts reaction.

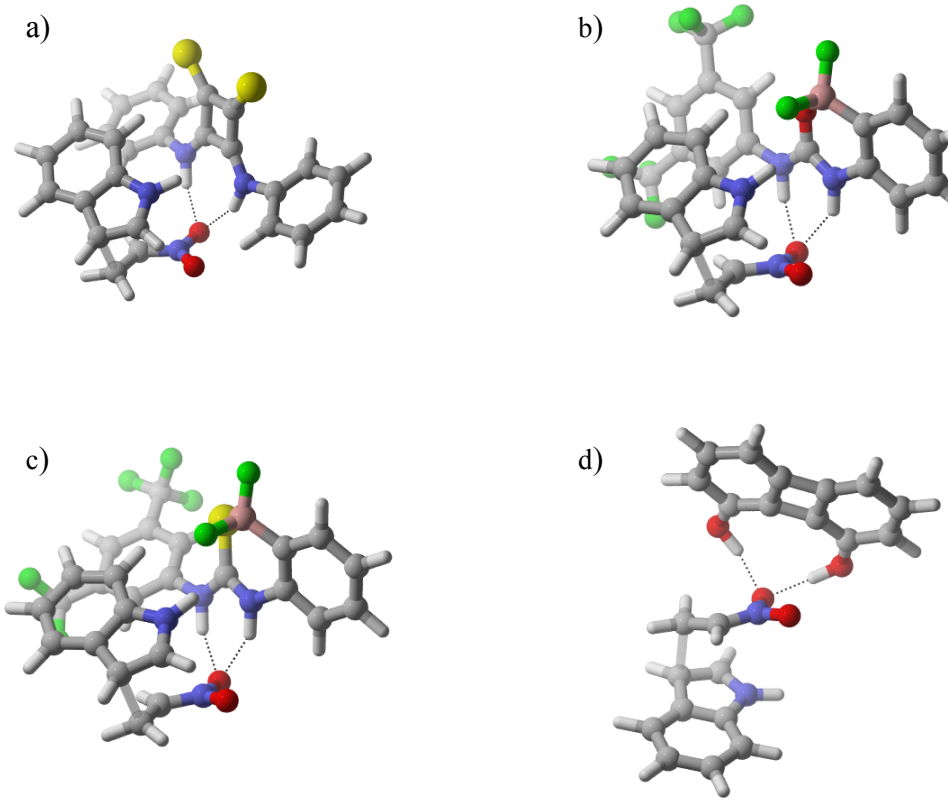

Figure 21. Friedel-Crafts TSs for catalysts (a) **4b**, (b) **8d**, (c) **8e**, and (d) **9** exhibiting the binding mode with one oxygen forming two hydrogen bonds.

Interestingly, while the HBCs in which only a single oxygen accepts both hydrogen bonds were always less favorable than ones in which both oxygens were involved in hydrogen bonding, this

was not the case for the TSs. In addition to **3c**, the lowest-lying TS for catalysts **4b**, **8d**, **8e**, and **9** all adopted binding modes in which one oxygen accepts both hydrogen bonds. The TSs for these four catalysts are shown in Figure 21. The twenty other lowest energy TSs adopted the twisted or planar binding mode.

The effects of different substituents on the activation barriers for the Diels-Alder and Friedel-Crafts reactions were analyzed by plotting the activation barrier ($\Delta G^{\ddagger}$) against the substituent for catalyst groups 1-6, as shown in Figure 22. The downward trend in activation energy versus substituents **a**, **b**, and **c** shows that adding aryl substituents and electron withdrawing groups increases the rate of the Diels-Alder and Friedel-Crafts reactions. Because this was seen earlier in Figure 13, we can conclude that a catalyst with substituent **c** will form stronger HBCs and catalyze the Diels-Alder or Friedel-Crafts reactions more than an analogous catalyst with substituent **a**.

Earlier, it was shown that substituents affected MVK-HBC strengths and NE-HBC strengths similarly. In contrast, the effects of substituents on the Diels-Alder activation barriers are very different from the effects of substituents on the Friedel-Crafts activation barriers. For example, sulfamide catalysts **5a**, **5b**, and **5c** catalyze the Diels-Alder reaction less effectively than any other catalyst with the same substituent. For the Friedel-Crafts reaction however, the sulfamide catalysts are more effective than urea and thiourea catalysts. More differences arise between the reactions, such as the effectiveness of urea catalysts compared to thiourea or squaramide catalysts.

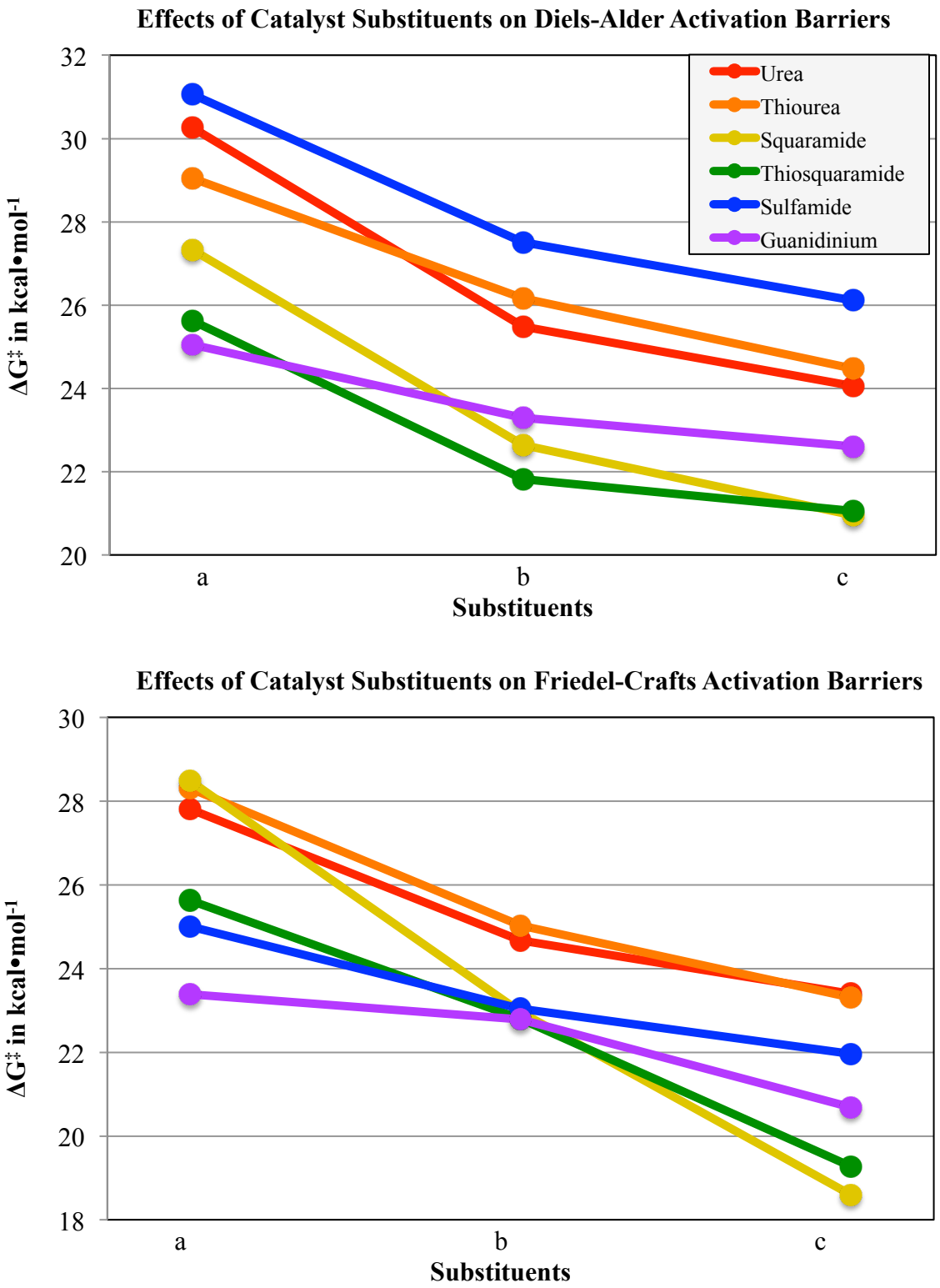

Figure 22. The effects of substituents a, b, and c on Diels-Alder and Friedel-Crafts activation barriers are plotted.

To explore the relationship between the Diels-Alder and Friedel-Crafts activation barriers, these data are plotted against eachother in Figure 23. The activation energies are weakly correlated with each other, and DHB catalysts do not affect Diels-Alder cycloadditions and Friedel-Crafts alkylations the same way qualitatively or quantitatively. As a result, few trends regarding catalytic efficacy can be made that apply to both reactions.

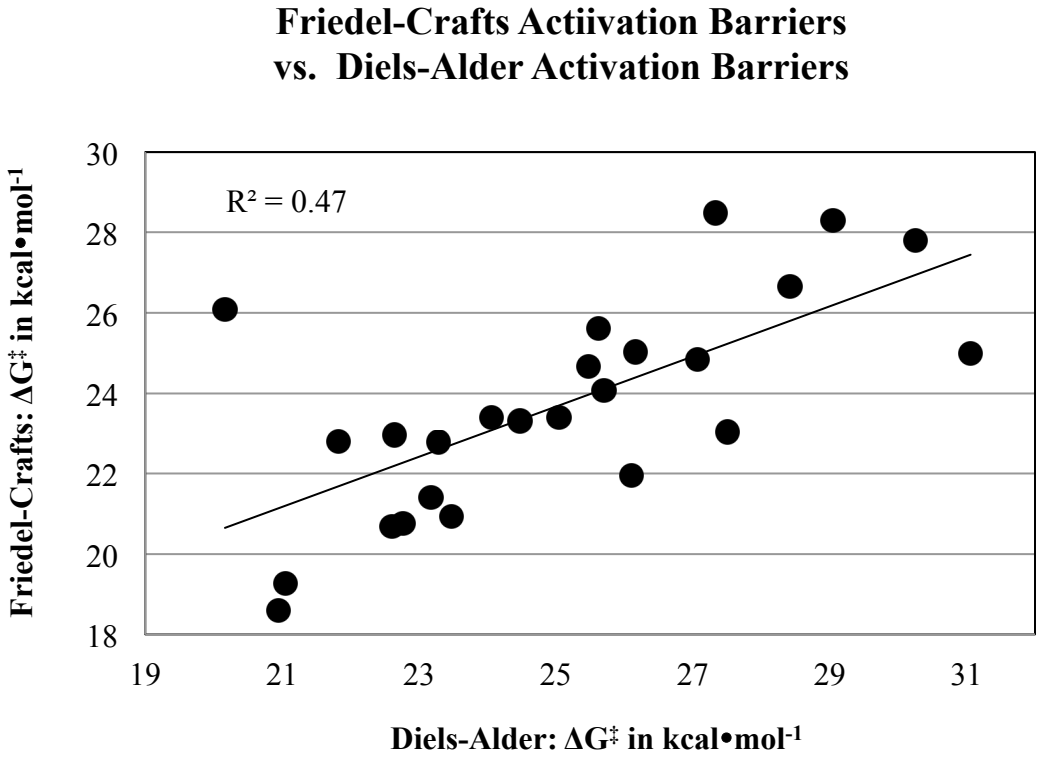

Figure 23. Comparison of Friedel-Crafts activation barriers and Diels-Alder activation barriers.

The ultimate goal of this study was to determine whether there is a relationship between HBC strengths and catalytic efficacy. activation barriers, $\Delta G^{\ddagger}$**,** are plotted again ΔG_{bind} for the Diels-Alder and Friedel-Crafts reactions in Figure 24. For the Diels-Alder reaction, there is a strong correlation between HBC strength and activation energy. Therefore, if a DHB organocatalyst forms strong HBCs with MVK, then it will most likely catalyze the Diels-Alder reaction

effectively. Therefore, one can rationally design more effective catalysts for the Diels-Alder reaction by increasing the strength of the corresponding HBC. It is important to note that strong correlation does not imply causation- that is, the strength of the HBC does not decide the efficacy of the catalyst. Instead, the relationship shows that HBC strength is dependent on the catalysts' activation mode. Dual hydrogen-bonding activates many substrates by shifting electron density from the substrate towards the catalyst, rendering them more susceptible to nucleophilic attack. Therefore, a stronger HBC removes more electron density from MVK, which increases the rate of the Diels-Alder cycloaddition.

Unlike the Diels-Alder reaction, the Friedel-Crafts reaction shows a weak correlation between HBC strength and activation energy. Thus, a catalyst that forms a stronger HBC will not necessarily be more efficient, and there is no basis in designing a DHB organocatalyst based on its NE-HBC strength.

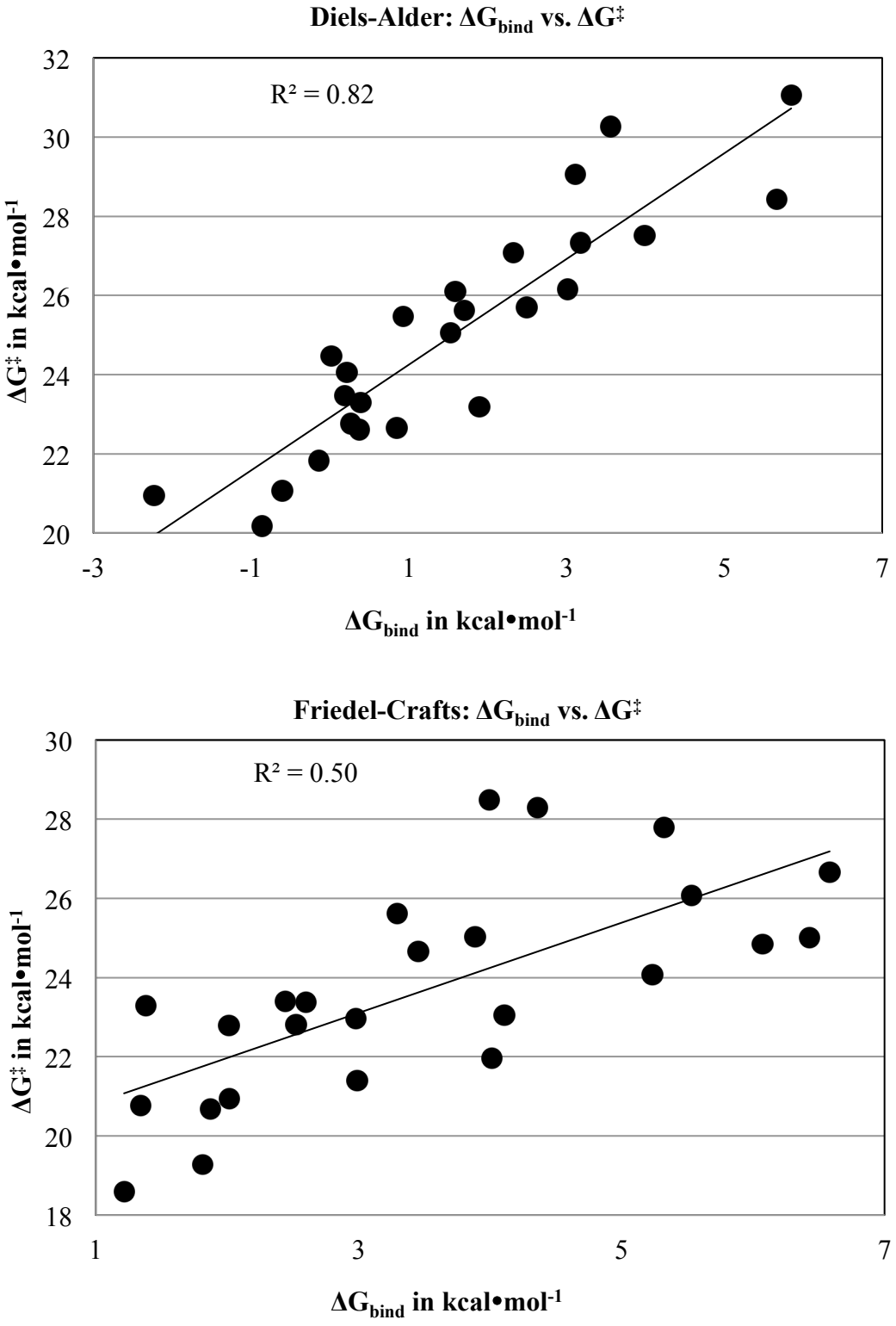

Figure 24. ΔG_{bind} versus $\Delta G^{\ddagger}$ for the Diels-Alder cycloaddition (top) and the Friedel-Crafts alkylation (bottom).

CHAPTER IV

CONCLUSION

Hydrogen bonding complexes and transition states for dual-hydrogen-bond catalyzed Diels-Alder and Friedel-Crafts reactions were studied using modern computational chemistry tools. We determined that the chromophore used by Kozlowski et al. cannot be used to quantify HBC strength, because it binds differently with the catalysts compared to MVK and NE.[9] Using a set of 25 model DHB organocatalysts, structural motifs that resulted in stronger HBCs were identified. For example, squaramides form stronger HBCs than analogous urea catalysts. Additionally, electron withdrawing substituents, such as 3,5-bis(trifluoromethyl)phenyl increase HBC strength. In fact, catalyst **3c**, which exhibits both motifs, formed the strongest HBCs with both substrates of the catalysts studied herein.

Then, we showed examples when the hypothesis from Lu and Wheeler that HBC strength was dependent on the N-H•••O bond angle, and Schreiner's suggestion that the 3,5-bis(trifluoromethyl)phenyl substituent increases HBC strength due to dispersion interactions involving the ortho-hydrogen are qualitatively incorrect.[27,28] Additionally, we showed that MVK-HBC binding energies are only weakly correlated with NE-HBC binding energies.

With regard to transition states, we found the most and least effective catalysts for both reactions. The most effective catalysts for the Diels-Alder and Friedel-Crafts reactions are **9** and **3c**, respectively. However, few predictive trends regarding catalytic efficacy could be made that apply to both reactions.

Finally, we determined that there is a strong correlation between HBC strength and activation energy for the Diels-Alder cycloaddition, but not for the Friedel-Crafts alkylation. Therefore, HBC strength is a metric that can justifiably be used to design DHB organocatalysts for the Diels-Alder cycloaddition, but not the Friedel-Crafts alkylation.

REFERENCES

(1) Dalko, P. I.; Moisan, L. Enantioselective organocatalysis. *Angew Chem Int Edit* **2001**, *40*, 3726-3748.

(2) MacMillan, D. W. C. The advent and development of organocatalysis. *Nature* **2008**, *455*, 304-308.

(3) Klare, H.; Neudorfl, J. M.; Goldfuss, B. New hydrogen-bonding organocatalysts: Chiral cyclophosphazanes and phosphorus amides as catalysts for asymmetric Michael additions. *Beilstein J. Org. Chem.* **2014**, *10*, 224-236.

(4) Aluminum Chloride; MSDS No. 563919 [Online]. http://www.sigmaaldrich.com/MSDS/MSDS/DisplayMSDSPage.do?country=US&language=en&productNumber=563919&brand=ALDRICH&PageToGoToURL=http%3A%2F%2Fwww.sigmaaldrich.com%2Fcatalog%2Fproduct%2Faldrich%2F563919%3Flang%3Den (accessed November 21 2015).

(5) Urea; MSDS No. U4883 [Online]. https://www.sigmaaldrich.com/MSDS/MSDS/DisplayMSDSPage.do?country=US&language=en&productNumber=U4883&brand=SIGMA&PageToGoToURL=https%3A%2F%2Fwww.sigmaaldrich.com%2Fcatalog%2Fproduct%2Fsigma%2Fu4883%3Flang%3Den (accessed Nov 21 2015).

(6) Jeffrey, G. A.: *An Introduction to Hydrogen Bonding*; Oxford University Press: New York, 1997.

(7) Schreiner, P. R. Metal-free organocatalysis through explicit hydrogen bonding interactions. *Chem. Soc. Rev.* **2003**, *32*, 289-296.

(8) Wittkopp, A.; Schreiner, P. R. Metal-free, noncovalent catalysis of Diels-Alder reactions by neutral hydrogen bond donors in organic solvents and in water. *Chem. Eur. J.* **2003**, *9*, 407-414.

(9) Walvoord, R. R.; Huynh, P. N. H.; Kozlowski, M. C. Quantification of Electrophilic Activation by Hydrogen-Bonding Organocatalysts. *J. Am. Chem. Soc.* **2014**, *136*, 16055-16065.

(10) Zhao, Y.; Truhlar, D. G. The M06 suite of density functionals for main group thermochemistry, thermochemical kinetics, noncovalent interactions, excited states, and transition elements: two new functionals and systematic testing of four M06-class functionals and 12 other functionals. *Theor. Chem. Acc.* **2008**, *120*, 215-241.

(11) Chai, J. D.; Head-Gordon, M. Long-range corrected hybrid density functionals with damped atom-atom dispersion corrections. *Phys. Chem. Chem. Phys.* **2008**, *10*, 6615-6620.

(12) Seeman, J. I. Effect of Conformational Change on Reactivity in Organic-Chemistry - Evaluations, Applications, and Extensions of Curtin-Hammett Winstein-Holness Kinetics. *Chem. Rev.* **1983**, *83*, 83-134.

(13) CYLview, 1.0b; Legault, C. Y. Université de Sherbrooke, 2009 (http://www.cylview.org).

(14) Jmol: an open-source Java viewer for chemical structures in 3D. (http://www.jmol.org).

(15) Johnson, E. R.; Keinan, S.; Mori-Sanchez, P.; Contreras-Garcia, J.; Cohen, A. J.; Yang, W. T. Revealing Noncovalent Interactions. *J. Am. Chem. Soc.* **2010**, *132*, 6498-6506.

(16) Contreras-Garcia, J.; Johnson, E. R.; Keinan, S.; Chaudret, R.; Piquemal, J. P.; Beratan, D. N.; Yang, W. T. NCIPLOT: A Program for Plotting Noncovalent Interaction Regions. *J. Chem. Theory Comput.* **2011**, *7*, 625-632.

(17) Houk, K. N.; Liu, P. Using Computational Chemistry to Understand & Discover Chemical Reactions. *Daedalus* **2014**, *143*, 49-66.

(18) Raju, R. K.; Bloom, J. W. G.; An, Y.; Wheeler, S. E. Substituent Effects on Non-Covalent Interactions with Aromatic Rings: Insights from Computational Chemistry. *ChemPhysChem* **2011**, *12*, 3116-3130.

(19) Wheeler, S. E. Controlling the local arrangements of pi-stacked polycyclic aromatic hydrocarbons through substituent effects. *Crystengcomm.* **2012**, *14*, 6140-6145.

(20) Wheeler, S. E.; Bloom, J. W. G. Toward a More Complete Understanding of Noncovalent Interactions Involving Aromatic Rings. *J. Phys. Chem. A* **2014**, *118*, 6133-6147.

(21) Wheeler, S. E.; Houk, K. N. Substituent effects in the benzene dimer are due to direct interactions of the substituents with the unsubstituted benzene. *J. Am. Chem. Soc.* **2008**, *130*, 10854-10855.

(22) Wheeler, S. E.; Houk, K. N. Origin of substituent effects in edge-to-face aryl-aryl interactions. *Mol. Phys.* **2009**, *107*, 749-760.

(23) An, Y.; Bloom, J. W. G.; Wheeler, S. E. Quantifying the pi-Stacking Interactions in Nitroarene Binding Sites of Proteins. *J. Phys. Chem. B* **2015**, *119*, 14441-14450.

(24) An, Y.; Raju, R. K.; Lu, T. X.; Wheeler, S. E. Aromatic Interactions Modulate the 5 '-Base Selectivity of the DNA-Binding Autoantibody ED-10. *J. Phys. Chem. B* **2014**, *118*, 5653-5659.

(25) Seguin, T. J.; Lu, T. X.; Wheeler, S. E. Enantioselectivity in Catalytic Asymmetric Fischer Indolizations Hinges on the Competition of pi-Stacking and CH/pi Interactions. *Org. Lett.* **2015**, *17*, 3066-3069.

(26) Wheeler, S. E.; McNeil, A. J.; Muller, P.; Swager, T. M.; Houk, K. N. Probing Substituent Effects in Aryl-Aryl Interactions Using Stereoselective Diels Alder Cycloadditions. *J. Am. Chem. Soc.* **2010**, *132*, 3304-3311.

(27) Lippert, K. M.; Hof, K.; Gerbig, D.; Ley, D.; Hausmann, H.; Guenther, S.; Schreiner, P. R. Hydrogen-Bonding Thiourea Organocatalysts: The Privileged 3,5-Bis(trifluoromethyl)phenyl Group. *Eur. J. Org. Chem.* **2012**, 5919-5927.

(28) Lu, T. X.; Wheeler, S. E. Origin of the Superior Performance of (Thio)Squaramides over (Thio)Ureas in Organocatalysis. *Chem. Eur. J.* **2013**, *19*, 15141-15147.

(29) Arunan, E.; Desiraju, G. R.; Klein, R. A.; Sadlej, J.; Scheiner, S.; Alkorta, I.; Clary, D. C.; Crabtree, R. H.; Dannenberg, J. J.; Hobza, P.; Kjaergaard, H. G.; Legon, A. C.; Mennucci, B.; Nesbitt, D. J. Defining the hydrogen bond: An account (IUPAC Technical Report). *Pure Appl. Chem.* **2011**, *83*, 1619-1636.

APPENDIX A

ΔG_{bind} and $\Delta G^{\ddagger}$ for Catalysts 1-12 with MVK and NE

Catalyst	$\Delta G_{bind,MVK}$ (kcal•mol^{-1})	$\Delta G_{bind,NE}$ (kcal•mol^{-1})	$\Delta G^{\ddagger}_{MVK}$ (kcal•mol^{-1})	$\Delta G^{\ddagger}_{NE}$ (kcal•mol^{-1})
1a	3.55	5.32	30.26	27.80
1b	0.93	3.45	25.48	24.67
1c	0.21	2.44	24.05	23.39
2a	3.11	4.36	29.05	28.30
2b	3.01	3.88	26.16	25.03
2c	0.02	1.38	24.47	23.30
3a	3.17	4.00	27.33	28.48
3b	0.84	2.98	22.64	22.96
3c	**-2.24**	**1.22**	20.95	**18.59**
4a	1.71	3.30	25.62	25.63
4b	-0.14	2.52	21.82	22.80
4c	-0.61	1.81	21.06	19.27
5a	5.85	6.43	31.06	25.00
5b	3.99	4.11	27.51	23.04
5c	1.59	4.02	26.11	21.96
6a	1.53	2.60	25.05	23.38
6b	0.39	2.01	23.29	22.78
6c	0.37	1.87	22.61	20.69
7	0.18	2.02	23.48	20.93
8d	0.26	1.34	22.76	20.77
8e	1.90	2.99	23.17	21.41
9	-0.87	5.53	**20.16**	26.08
10	2.49	5.23	25.70	24.08
11	2.33	6.07	27.07	24.84
12	5.66	6.58	28.42	26.65